Journal of Power Sources 195 (2010) 445–452

Contents lists available at ScienceDirect

Journal of Power Sources

journal homepage: www.elsevier.com/locate/jpowsour

Highly stable Pt and PtPd hybrid catalysts supported on a nitrogen-modified carbon composite for fuel cell application☆

Xuguang Li, Sehkyu Park, Branko N. Popov*

Center for Electrochemical Engineering, Department of Chemical Engineering, University of South Carolina, Columbia, SC 29208, USA

ARTICLE INFO

Article history:
Received 17 April 2009
Received in revised form 12 June 2009
Accepted 14 July 2009
Available online 22 July 2009

Keywords:
Durability
Catalyst
Support
Cathode
Fuel cell

ABSTRACT

The durability and cost of fuel cell cathode catalysts are major technical barriers to the commercialization of fuel cells for vehicle applications. In this work, novel Pt and PtPd hybrid catalysts are developed that use a nitrogen-modified carbon composite (NMCC), which is itself active for the oxygen reduction reaction (ORR), instead of a conventional carbon black support. The fuel cell accelerated stress test (AST) for supports and catalysts demonstrated that the Pt_3Pd_1/NMCC and Pt/NMCC hybrid catalysts possess much higher stability than Pt/C catalysts in polymer electrolyte membrane (PEM) fuel cells. Moreover, the hybrid catalysts exhibit higher mass activity than the Pt/C catalysts. The origin of the hybrid catalysts' improved performance relative to Pt/C is discussed in light of pore size distribution and surface area analysis, XRD, XPS, and TEM analyses and electrochemical measurements.

Published by Elsevier B.V.

1. Introduction

Carbon-supported platinum (Pt/C) and platinum-based alloy catalysts are the most commonly used cathode catalysts for polymer electrolyte membrane (PEM) fuel cells. Alloying Pt with other transition metals, such as Co, Fe, and Cr, can increase the catalytic activity and sometimes the stability of these catalysts for the oxygen reduction reaction (ORR). This effect may be attributed to the formation of alloys with favorable Pt–Pt interatomic distances or Pt crystal orientations in the Pt alloys that facilitate oxygen reduction and mitigate Pt sintering/dissolution [1–4].

Considerable effort has been devoted to the development of carbon-supported Pt-based catalysts. However, the stability and cost of these catalysts are still major technical barriers to the commercialization of fuel cells for vehicle applications. The durability of Pt-based catalysts can be compromised by Pt sintering and dissolution, especially under the load cycling found in fuel cell vehicles, which accelerates these processes [5–10]. These effects significantly decrease the electrochemically active surface area and Pt utilization in fuel cell cathodes. In addition, the dissolution of non-noble metals in the catalyst alloy not only causes a decrease in the catalyst's activity, but it also poisons the membrane electrode assemblies (MEAs) via ion exchange between the metal cations and the protonic sites on both the Nafion membrane and the ionomer inside the catalyst layer [8].

Another concern complicating the use of carbon-supported Pt-based catalysts is the corrosion of the high surface area carbon support [10–14]. During the startup/shutdown cycle, the cathode potential of a vehicle's fuel cells may increase to 1.2–1.5 V, or even higher. The corrosion rate of carbon increases drastically at high electrode potentials, and can result in severe degradation of the carbon support via the following reaction:

$$C + 2H_2O \rightarrow CO_2 + 4H^+ + 4e^- \qquad E^0 = 0.207\,\text{Vvs.RHE}$$

Oxidation of the carbon surface increases its hydrophilicity and thus affects water removal, resulting in an increased mass transfer resistance. In addition, the oxidation of carbon increases the electrical resistance of the catalysts, leads to the aggregation of catalyst particles, and even damages the structure of the catalyst layer. In particular, platinum increases the corrosion rate of carbon supports [10–12].

Durability issues aside, the cost of Pt-based catalysts is another obstacle to the development of fuel cell vehicles due to the world's limited Pt reserves. Therefore, many recent studies have focused on decreasing Pt loadings and increasing Pt utilization in fuel cell electrodes while maintaining satisfactory activity and stability. These efforts include the design of novel catalysts, the use of new supporting materials, the development of new methods for catalyst synthesis, and the optimization of electrode structure and fabrication methods [13–19]. However, it is still challenging to obtain a

☆ Submitted as a technical paper to Journal of Power Sources, Dr. C.K. Dyer, Regional Editor for N. & S. America, Compact Power Inc., 16 Seven Oaks Circle, Madison, New Jersey 07940-1314, USA.

* Corresponding author. Tel.: +1 803 777 7314; fax: +1 803 777 8265.
E-mail address: popov@cec.sc.edu (B.N. Popov).

0378-7753/$ – see front matter. Published by Elsevier B.V.
doi:10.1016/j.jpowsour.2009.07.029

Pt-based fuel cell cathode catalyst with both good durability and high mass activity.

In the past four decades, low-cost non-precious metal catalysts for the ORR have been widely studied as alternatives to Pt. These catalysts can be prepared from transition metal macrocycles or transition metal-, nitrogen-, and carbon-based precursors. However, the nature of active sites in the non-precious metal catalysts is still a subject of controversy. One of the most accepted hypothesis is the metal-N_4/N_2 moiety bound to carbon substrate plays an important role toward ORR [20–22]. Another hypothesis is that the graphitic (quaternary) and pyridinic nitrogen doped on the carbon substrate's surface is an active site for oxygen reduction. The transition metal is not part of the active sites, but rather serves primarily to facilitate the incorporation of nitrogen into the graphitic carbon during the pyrolysis. The remaining metal particles are encased in the carbon substrate [23–30]. Our group has developed a nitrogen-modified carbon composite (NMCC) catalyst, which is prepared by the pyrolysis of a carbon-supported cobalt and/or iron nitrogen chelate followed by an acid leaching treatment [27–30].

In this work, we intend to detailedly investigate the hybrid catalysts by supporting the Pt (or PtPd) on the NMCC instead of a conventional carbon black substrate. These novel catalysts will contain nitrogen-doped sites and Pt sites, both of which are active for the ORR. Thus, we refer to them as hybrid catalysts. In addition to its possible own contribution to the overall activity (an advantage over a conventional carbon support), the NMCC is expected to improve the stability of hybrid catalysts through some synergistic effects. Our preliminary work has demonstrated that the NMCC-supported Pt catalyst exhibit a slightly higher mass activity than the conventional PtCo catalyst. The long-term stability measured at a constant current density of 1 A cm^{-2} and the electron probe microanalysis (EPMA) showed that the new catalyst is more stable than the conventional counterpart [30]. It was attributed to the application of a new synthesis methodology with Pt deposition on the Co-encased carbon substrate instead of the conventional synthesis routes involving Co deposition on Pt/C. The goal of this work is further examine and compare the effects of the new supporting material and further the third metal additive on the stability of catalyst support and catalyst, respectively. The fuel cell component accelerated stress tests (AST) are used to isolate the degradation of catalyst support and catalyst, and thus evaluate the individual stability of the catalyst support and catalyst in the Pt/NMCC, PtPd/NMCC, and Pt/C. Pore size distribution and BET surface area analysis, X-ray diffraction (XRD), X-ray photoelectron spectroscopy (XPS), and transmission electron microscopy (TEM), as well as electrochemical measurements, were used to characterize the catalyst supports and catalysts.

2. Experimental

2.1. Catalyst synthesis

The synthesis of the nitrogen-modified carbon composite (NMCC) catalyst was carried out according to the previously reported procedure [27–30]. Briefly, ethylene diamine was added to a $Co(NO_3)_2$ solution, followed by the addition of carbon black. The reaction mixture was refluxed at 85 °C for 4 h and then dried using a rotary evaporator at 80 °C under reduced pressure. The dried sample was heated to 700 °C under an Ar atmosphere at 8.8 MPa for 3 h. The heat-treated sample was treated with 0.5 M H_2SO_4 to remove excess Co on the carbon catalyst's surface.

The Pt/NMCC hybrid catalyst (20 wt% Pt) was prepared by depositing Pt on a NMCC support and then heating it to 800 °C in an Ar atmosphere. The PtPd/NMCC hybrid catalysts (20 wt% (Pt + Pd)) were synthesized by the successive deposition of Pd and Pt on a NMCC support followed by heating to 800 °C in an Ar atmosphere. The atomic ratio of Pt to Pd in the PtPd/NMCC catalysts varied from 7:1 to 1:3. For comparison, a Pt/C (20 wt% Pt) catalyst with a conventional carbon black support was also prepared. The bulk compositions of the catalysts were confirmed by the atomic absorption spectroscopy (AAS).

2.2. Rotating disk electrode (RDE) measurements

RDE measurements were performed in a standard three-compartment electrochemical cell. A glassy carbon disk (5.61 mm diameter) was used as the working electrode, a saturated mercury–mercury sulfate electrode was used as the reference electrode, and platinum foil was used as the counter electrode. A 0.5 M H_2SO_4 solution was used as the electrolyte. All potentials in this work are referenced to a relative hydrogen electrode (RHE). The catalyst ink was prepared by blending 24 mg of the catalyst with 3 mL of isopropyl alcohol. The ink (15 μL) was then deposited onto the glassy carbon. Nafion (5 μL of a 0.25 wt% solution) was applied to the catalyst layer to ensure good adhesion of the catalyst to the glassy carbon.

2.3. Fuel cell accelerated stress tests (AST) for supports and catalysts

The catalyst ink was prepared by ultrasonically mixing the catalyst with the Nafion solution and isopropyl alcohol for 2 h. The cathode's noble metal loading was 0.4 mg cm^{-2} and the anode's Pt loading was 0.5 mg cm^{-2}. The anode and cathode were hot-pressed to a Nafion 112 membrane at 140 °C under 15 atm for 3 min. The fuel cell was conditioned for about 15 h until the current density was constant. The electrochemical measurements were carried out in a single cell at 80 °C and an absolute pressure of 150 kPa. Pure hydrogen and air were supplied to the anode and cathode compartments, respectively. Polarization curve tests were conducted in constant stoichiometry mode using a 0.1 A cm^{-2} current step and a 20 min dwell time. The geometric area of the MEA was 25 cm^2.

Fuel cell accelerated stress tests of the support were performed as follows: (i) measure the initial polarization curve under H_2/air (relative humidity, RH = 50%; $\lambda(H_2)/\lambda(air) = 3/3$), (ii) hold at 1.2 V at 80 °C under an H_2/N_2 atmosphere (RH = 100%) for a period of time (*Note*: carbon corrosion is severe at high potential.), (iii) measure the air polarization curves again.

Fuel cell accelerated stress tests of the catalyst were performed as follows: (i) measure the initial polarization curve under an H_2/air atmosphere (RH = 100%; $\lambda(H_2)/\lambda(air) = 3/3$), (ii) potential cycle between 0.7 V for 30 s and 0.9 V for 30 s under an H_2/N_2 atmosphere (RH = 100%) (*Note*: Pt sintering and dissolution are severe under potential cycling conditions.), (iii) measure the air polarization curves again.

2.4. Physical and chemical characterizations

The BET surface areas and pore size distribution of the catalyst supports were measured by using NOVA 2000 high-speed surface area and pore size analyzer. The XRD patterns were recorded with an automated Rigaku diffractometer using Cu Kα radiation over a scanning angle range of 20–75° with a scan rate of 1.5° min^{-1}. XPS measurements were carried out on a Kratos AXIS Ultra DLD XPS system equipped with a hemispherical energy analyzer and a monochromatic Al Kα source, which was operated at 15 keV and 150 W. To determine the particle size of the catalysts, TEM was carried out using a high-resolution JEOL 2010F TEM system operated with LaB_6 filament at 200 kV.

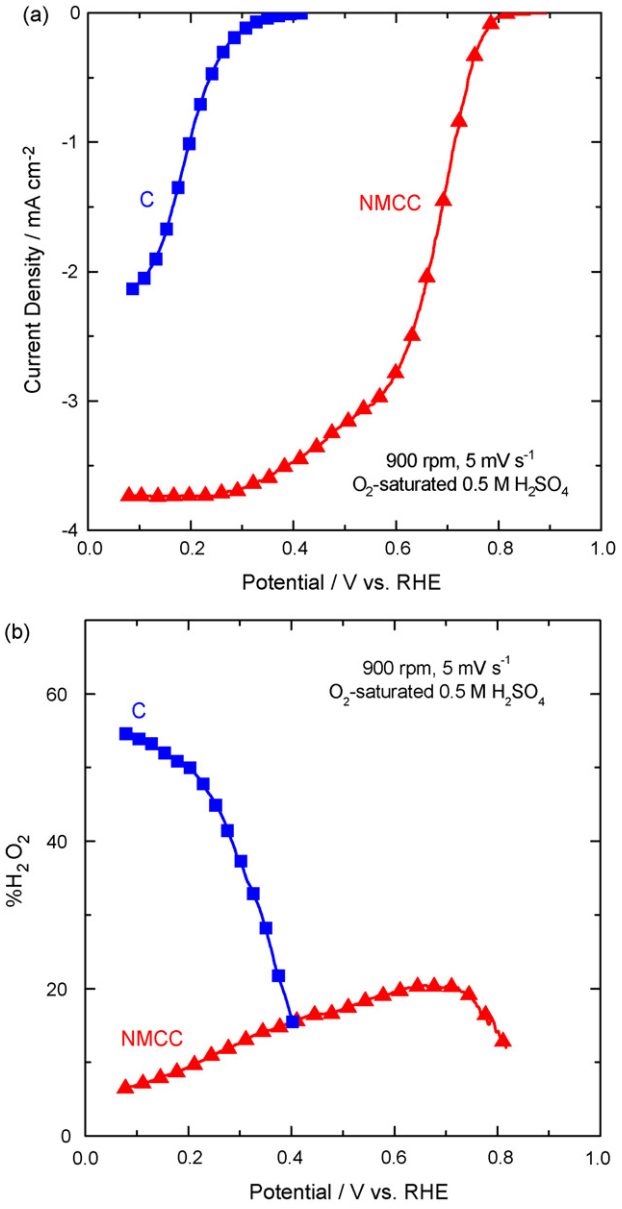

Fig. 1. (a) Polarization curves for the oxygen reduction reaction and (b) the percentages of H_2O_2 formed during the oxygen reduction reaction in O_2-saturated 0.5 M H_2SO_4 on the carbon black and nitrogen-modified carbon composite. Scan rate: 5 mV s^{-1}, rotation rate: 900 rpm.

3. Results and discussion

3.1. Comparison of nitrogen-modified carbon composite and carbon black

Fig. 1a shows the polarization curves for the oxygen reduction reaction in an O_2-saturated 0.5 M H_2SO_4 solution on the carbon black and nitrogen-modified carbon composite (NMCC) electrodes at a scan rate of 5 mV s^{-1} and a rotation rate of 900 rpm. The onset potential of the ORR on the carbon black electrode is only approximately 0.4 V, while it is approximately 0.82 V on the NMCC electrode, which also exhibits a limiting current plateau. Fig. 1b shows the percentage of H_2O_2 generated during the oxygen reduction on the carbon black and NMCC electrodes. It is evident that the amount of H_2O_2 produced on the NMCC during the oxygen reduction is much lower than that on the carbon black. The H_2O_2 is corrosive toward the carbon materials and is able to cause the oxidative destruction of the active sites and the defect sites in the fuel cell catalysts and supports [31,32].

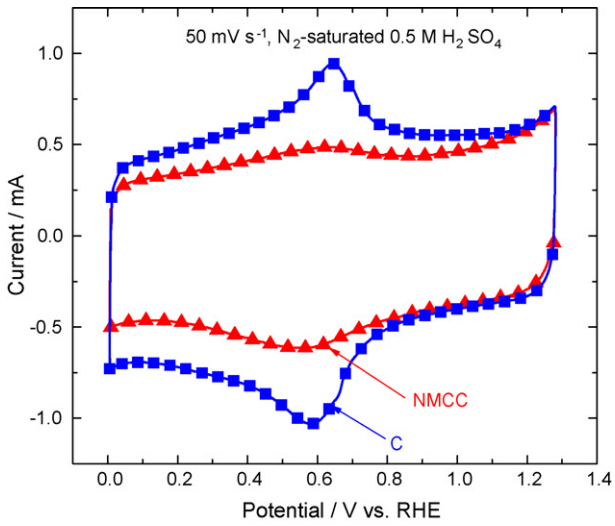

Fig. 2. Cyclic voltammograms of the carbon black and nitrogen-modified carbon composite in N_2-saturated 0.5 M H_2SO_4. Scan rate: 50 mV s^{-1}.

Fig. 2 shows the cyclic voltammograms of the carbon black and nitrogen-modified carbon composite. The measurements were performed in a N_2-saturated 0.5 M H_2SO_4 solution at a potential scan rate of 50 mV s^{-1}. A pair of redox peaks at about 0.6 V, which are associated with the quinine–hydroquinone couple, was observed for both the carbon black and NMCC. The intensity of the surface groups on the NMCC is lower in comparison with the carbon black due to a series of adsorption and deposition processes of the reactants onto the carbon substrate as well as the pyrolysis and leaching treatment. However, the capacitance of the NMCC and carbon black is similar, revealing they have similar porosity [33]. In addition, no redox peak corresponding to the cobalt species was observed in the CV of the NMCC, indicating that cobalt is not present on the surface of the NMCC.

Table 1 presents the BET surface areas of the carbon black and NMCC, and the respective contribution from the micropores and mesopores. It can be seen that subject to the adsorption, deposition, pyrolysis, and leaching treatment, the NMCC lost only 6% of surface area in comparison with the carbon black, which is mainly caused by the decrease of micropores. Fig. 3 shows the pore size distribution of the carbon black and NMCC. It is evident that the carbon black and NMCC have the similar pore size distribution centering at about 3–4 and 40–45 nm with a slightly positive shift for the NMCC. It can be concluded that the NMCC has the similar porosity with the carbon black, which is consistent with the aforementioned CV results. While preparing the Pt or Pt-based catalysts, the mesopores (pore diameters of 2–50 nm) of support are accessible for the reactants, which are the main location of the resultant catalyst particles, while the micropores (diameters smaller than 2 nm) are inaccessible. Therefore, the NMCC is a qualified support for the Pt-based catalysts.

Fig. 4 shows the XRD patterns of the carbon black and nitrogen-modified carbon composite. The broad characteristic diffraction peaks of C (0 0 2) and (1 0 1) were observed for the carbon black.

Table 1
BET surface areas of the carbon black and NMCC.

Support	BET surface area ($m^2\ g^{-1}$)	Area from micropores ($m^2\ g^{-1}$)	Area from mesopores ($m^2\ g^{-1}$)
C	808.8	262.5	546.3
NMCC	761.6	221.2	540.4

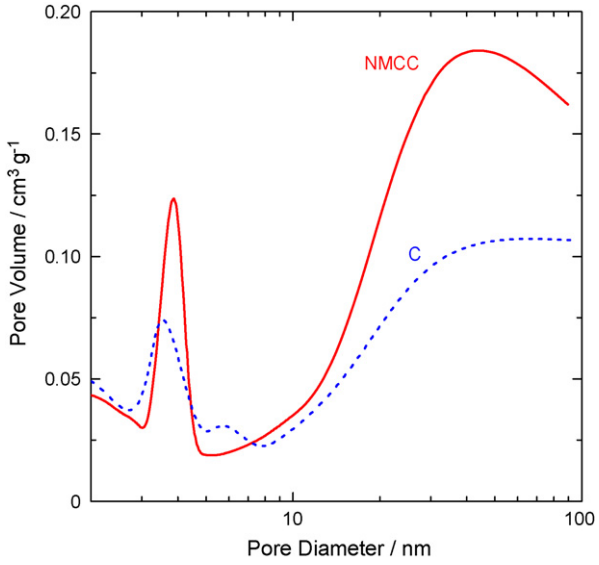

Fig. 3. Pore size distribution of the carbon black and nitrogen-modified carbon composite.

For the NMCC, the peak of C (0 0 2) becomes sharper and shifts positively, which is attributed to an increased graphitization of carbon and a doping of nitrogen in the carbon matrix [34,35]. The similar phenomenon was also reported in our previous study on the non-precious metal catalysts by XRD and TEM characterizations. The remaining cobalt with the diffraction peaks of Co (1 1 1) and (2 0 0) in the XRD pattern was observed to be covered with the graphitic carbon layers by the TEM [29]. In addition, Ozkan and co-workers also obtained the nanostructured nitrogen-modified carbon-based catalyst for ORR with high graphitization [25,26]. It is well known that the graphitized carbon materials are more thermally and electrochemically stable than the conventional carbon black. However, the graphitization often significantly decreases the porosity and surface area of carbon, which has an adverse effect on the subsequent dispersion of Pt or Pt-based particles. In our case, the NMCC maintain the relatively high porosity and surface area while increasing the graphitization level.

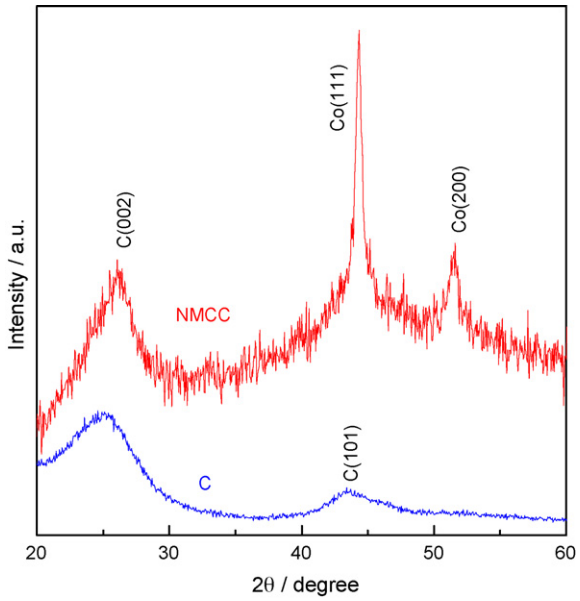

Fig. 4. XRD patterns of the carbon black and nitrogen-modified carbon composite.

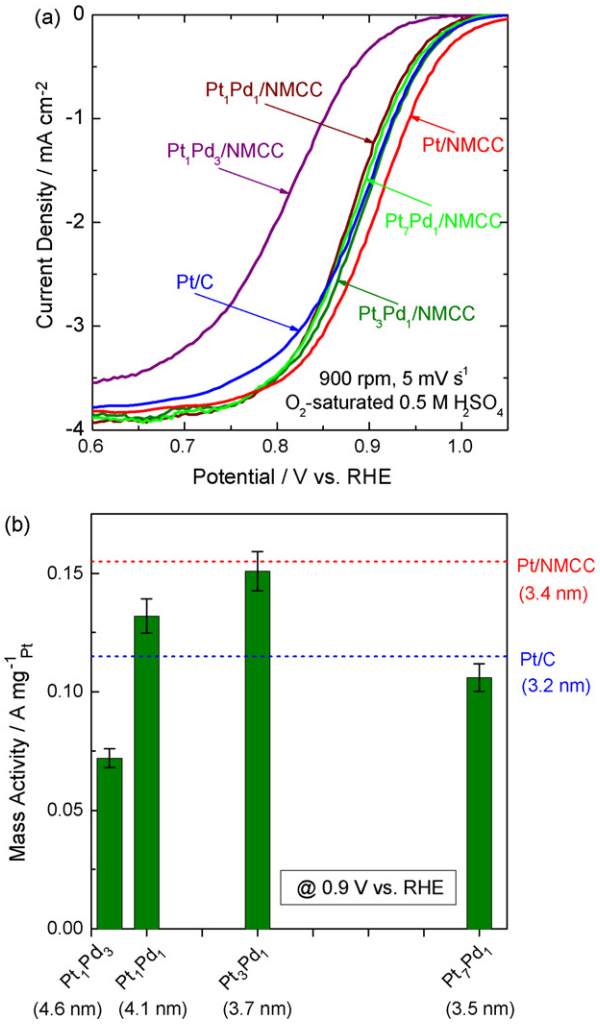

Fig. 5. (a) Polarization curves for the oxygen reduction reaction in O_2-saturated 0.5 M H_2SO_4 on the Pt/C catalyst, Pt/NMCC hybrid catalyst, and PtPd/NMCC hybrid catalysts with different Pt/Pd atomic ratios. Scan rate: 5 mV s^{-1}, rotation rate: 900 rpm. (b) Mass activity for the oxygen reduction reaction at 0.9 V on the PtPd/NMCC hybrid catalysts with different Pt/Pd atomic ratios. The data from the Pt/C catalyst and the Pt/NMCC hybrid catalyst are presented for comparison.

3.2. Electrochemical and physicochemical characterizations of Pt/NMCC, PtPd/NMCC, and Pt/C catalysts

Fig. 5a shows the polarization curves for the oxygen reduction reaction in an O_2-saturated 0.5 M H_2SO_4 solution on the Pt/C catalyst, Pt/NMCC hybrid catalyst, and PtPd/NMCC hybrid catalysts with varying Pt/Pd atomic ratios at a scan rate of 5 mV s^{-1} and a rotation rate of 900 rpm. Mixed kinetic-diffusion control regions from 0.8 to 1.0 V and onset-potentials of up to 1.05 V were observed for all catalysts except for the Pt_1Pd_3/NMCC catalyst. For clarity, the mass activity (MA) at 0.9 V of the PtPd/NMCC hybrid catalysts with different Pt/Pd atomic ratios is illustrated in Fig. 5b. The mass activity (kinetic current density, A $mg^{-1}{}_{Pt}$) is made with respect to the Pt loading on the RDE. The kinetic current, i_k is given in terms of the current after a correction for diffusion effects using the equation:

$$i_k = \frac{i_l i}{i_l - i} \quad (1)$$

where i_l is the limiting current and i is the measured current. For accuracy, an error bar is given to the mass activity of the PtPd catalysts. The average values of the mass activity of the Pt/C and Pt/NMCC are also presented for comparison.

As shown in Fig. 5b, the mass activity of the PtPd/NMCC hybrid catalysts for the ORR achieves a maximum at a Pt/Pd atomic ratio of 3/1, which is comparable with the Pt/NMCC. Further increases in the Pd content caused the decrease of the activity of the PtPd catalysts and thus the Pt_1Pd_3 exhibits a minimum value. In conclusion, the Pt/NMCC and Pt_3Pd_1/NMCC hybrid catalysts show higher catalytic activity than the conventional Pt/C catalyst. It is well known that the mass activity of Pt/C for ORR goes through a maximum at ca. 3–4 nm of Pt particles due to the particle size effect on the kinetics of ORR [36–40]. In this work, the average particle sizes of the catalysts calculated from the TEM were presented in the parenthesis under the catalyst names in Fig. 5b. As can be seen, the mass activity the PtPd hybrid catalysts go through a maximum at the particle size of 3.7 nm (Pt_3Pd_1). This tendency is consistent with that in the literatures [36–40]. Therefore, the particle size effect may at least partially explain the relationship between the mass activity of PtPd catalysts and the Pt/Pd ratios. Besides the particle size effect, the minimum activity of Pt_1Pd_3 may be attributed to the blocking of Pt active sites by a large amount of Pd in the catalyst. The activity difference between Pt_3Pd_1/NMCC, Pt/NMCC, and Pt/C is more likely the combined consequence of the particle size effect and the alloying effect. Their difference in the alloying level and/or structure will be demonstrated in the following XRD and XPS analyses. On the other hand, it can be seen that most of the NMCC-supported catalysts except Pt_1Pd_3 and Pt_1Pd_1 with a high Pd content, exhibit the comparable particle sizes with the Pt/C. This confirms that the NMCC is a suitable support for preparing high-dispersion Pt or Pt-based catalysts with small particle sizes.

Fig. 6 shows the XRD patterns of the Pt/C catalyst, Pt/NMCC hybrid catalyst, and Pt_3Pd_1/NMCC hybrid catalyst. The Pt/C catalyst has peaks at 39.7°, 46.2°, and 67.6°, which are the characteristic diffraction peaks for face centered cubic crystalline Pt (1 1 1), (2 0 0), and (2 2 0), respectively. However, the positions of these diffraction peaks in the Pt/NMCC hybrid catalyst are obviously shifted to higher 2θ values. This indicates the formation of a PtCo alloy in the Pt/NMCC hybrid catalyst, which is attributed to some of the cobalt encased in the carbon matrix being incorporated into the Pt lattice. In the case of the Pt_3Pd_1/NMCC catalyst, a positive shift of the Pt peaks was also observed, but the magnitude of the shift is smaller

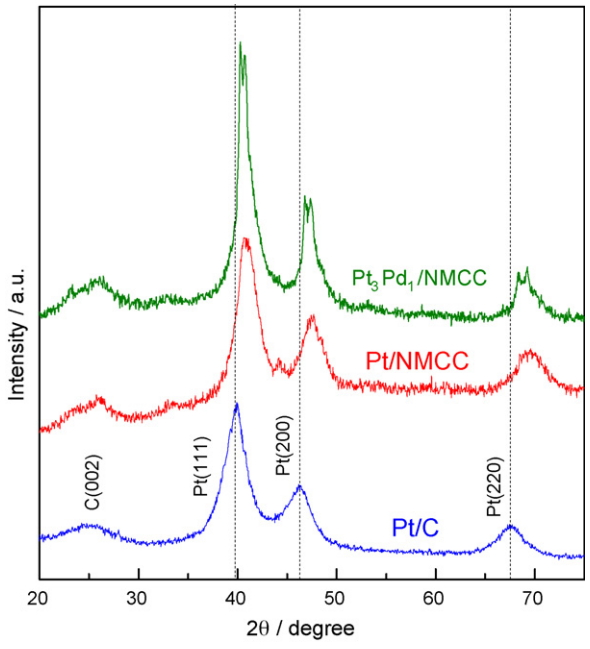

Fig. 6. XRD patterns of the Pt/C catalyst, Pt/NMCC hybrid catalyst, and Pt_3Pd_1/NMCC hybrid catalyst.

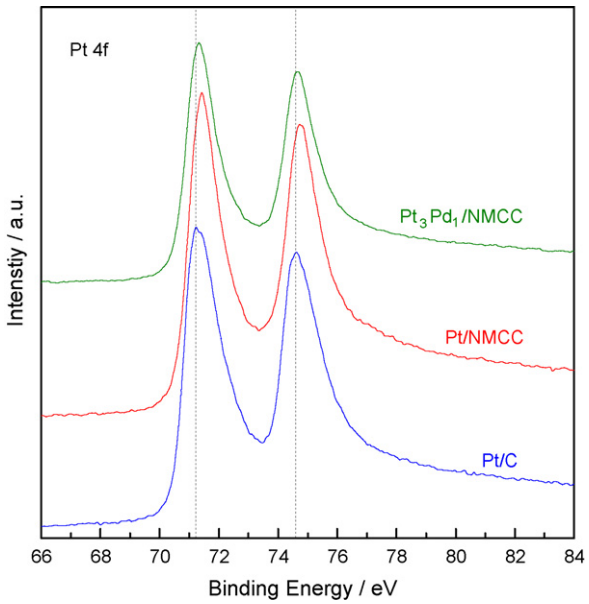

Fig. 7. XPS core level spectra for the Pt 4f orbitals of the Pt/C catalyst, Pt/NMCC hybrid catalyst, and Pt_3Pd_1/NMCC hybrid catalyst.

than that observed in the Pt/NMCC catalyst. This indicates that the extent of alloying and/or the structures in the Pt_3Pd_1/NMCC are different from that in the Pt/NMCC catalyst due to the addition of Pd between the Pt and the NMCC. The alloying difference can be at least one of the reasons accounting for the mass activity differences shown in Fig. 5. In addition, it may also affect the stability of the catalysts [1–4,41]. In Fig. 6, the diffraction peak at about 25.0° is attributed to C (0 0 2) of the support. In comparison with the Pt/C, the C (0 0 2) diffraction peaks in the Pt/NMCC and Pt_3Pd_1/NMCC hybrid catalysts are sharper, which indicates that the extent of graphitization in the NMCC is higher than that in the conventional carbon black. This confirms the XRD analysis of the carbon black and NMCC shown in Fig. 4. During the preparation of the NMCC, the presence of a transition metal effectively decreases the graphitization temperature of carbon black. Graphitization generally leads to reduced surface heterogeneity and thus increases corrosion resistance. However, graphitization only slows the kinetics of the carbon oxidation reaction; it does not change the fundamental oxidation mechanisms [12,13].

Fig. 7 shows the XPS core level spectra for the Pt 4f orbitals of the Pt/C catalyst, Pt/NMCC hybrid catalyst, and Pt_3Pd_1/NMCC hybrid catalyst. We observed that the Pt 4f peaks of the Pt/NMCC catalyst shift to higher energies relative to the Pt/C catalyst [41,42]. The positive shift in the Pt_3Pd_1/NMCC catalyst's Pt 4f peak is not as large as observed with the Pt/NMCC. It is interesting that this tendency is consistent with the XRD result, which confirmed that the addition of Pd between the Pt and the NMCC can alter the catalysts' surface/structure properties. This may result in the activity and stability difference of the catalysts.

3.3. *Fuel cell accelerated stress tests (AST) for supports and catalysts in Pt/NMCC, Pt_3Pd_1/NMCC, and Pt/C*

Fig. 8a shows the H_2-air fuel cell polarization curves using the Pt/C catalyst, Pt/NMCC hybrid catalyst, and Pt_3Pd_1/NMCC hybrid catalyst before and after 50 h of the accelerated stress test on the support. In the test, the fuel cell cathode is held at 1.2 V for 50 h, since carbon corrosion is accelerated at high electrode potentials. The initial fuel cell polarization curves indicated that both the Pt_3Pd_1/NMCC and Pt/NMCC hybrid catalysts have higher catalytic

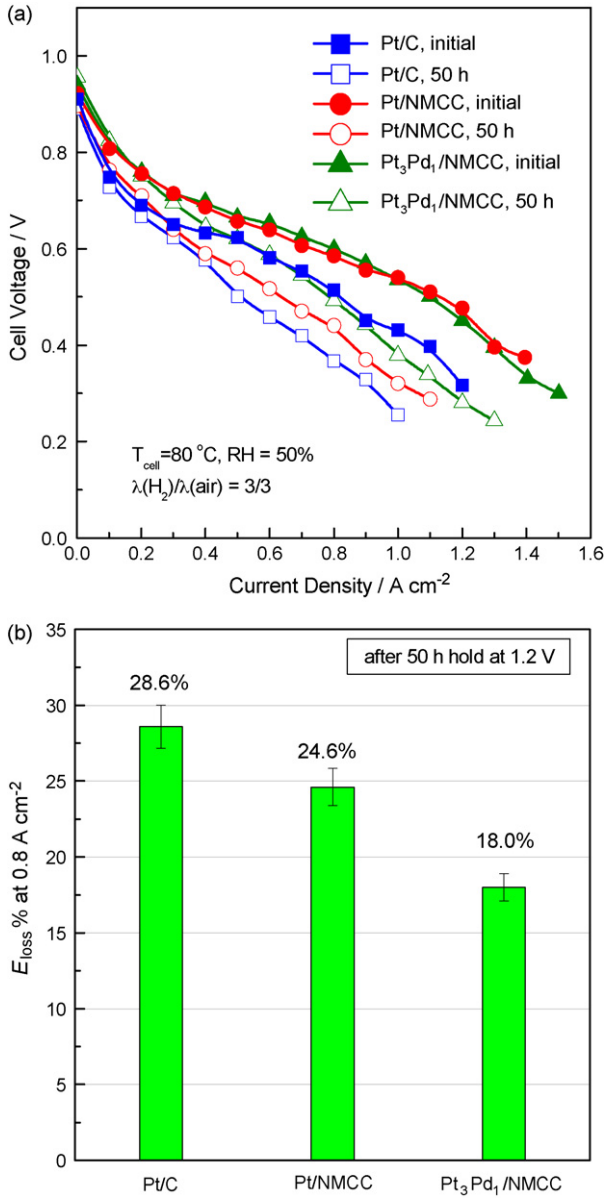

Fig. 8. (a) H_2-air fuel cell polarization curves using the Pt/C catalyst, PtPd/NMCC hybrid catalyst, and Pt_3Pd_1/NMCC hybrid catalyst before and after 50 h of the accelerated stress test on the support. (b) Percentage of fuel cell potential loss at 0.8 A cm^{-2} before and after 50 h of the accelerated stress test on the support.

performance than the Pt/C system. After 50 h of the accelerated support corrosion test at 1.2 V, the Pt_3Pd_1/NMCC catalyst exhibits much better polarization performance than either the Pt/NMCC or the Pt/C systems. In order to clearly demonstrate the extent of the support's degradation, the percentage of fuel cell potential loss (E_{loss}%) at 0.8 A cm^{-2} after 50 h of the support corrosion test is presented in Fig. 8b. The E_{loss}% is expressed as:

$$E_{loss}\% = \left(\frac{E_{ini} - E}{E_{ini}}\right) \times 100\% \quad (2)$$

where E_{ini} and E denote the initial potential and the potential measured after 50 h of the carbon corrosion test at 0.8 A cm^{-2}, respectively. For accuracy, the error bar is given to the histogram data and the average value of performance loss is also presented in Fig. 8b. The degradation in the catalyst supports changes in the following sequence: Pt/C > Pt/NMCC > Pt_3Pd_1/NMCC. First, this indicates that the NMCC support is much more stable than the conventional carbon black support, which may be due to the higher degree of graphitization in the NMCC, as demonstrated by the XRD results of the supports and catalysts (see Figs. 4 and 6). Second, the corrosion test result demonstrates that the addition of an appropriate amount of a third metal, Pd, to the Pt_3Pd_1/NMCC hybrid catalyst further enhances the stability of the NMCC support. According to the literatures [10–12], the Pt-catalyzed carbon corrosion may be at least partially mitigated by the presence of Pd between the carbon and Pt. However, further increase in the Pd content of the hybrid catalysts, such as Pt_1Pd_1/NMCC, did not result in further increases in the support's durability (data not shown). This may be attributed to the instability of Pd ($E^0_{Pd^{2+}/Pd} = 0.915$ V, $E^0_{Pd0/Pd} = 0.79$ V) under corrosive conditions, such as low pH, high temperature, high water content, high potential, and high oxygen concentration [43–49]. In the case of the Pt_3Pd_1/NMCC system, the Pd may be mostly covered by Pt, and thus is protected from oxidation/corrosion.

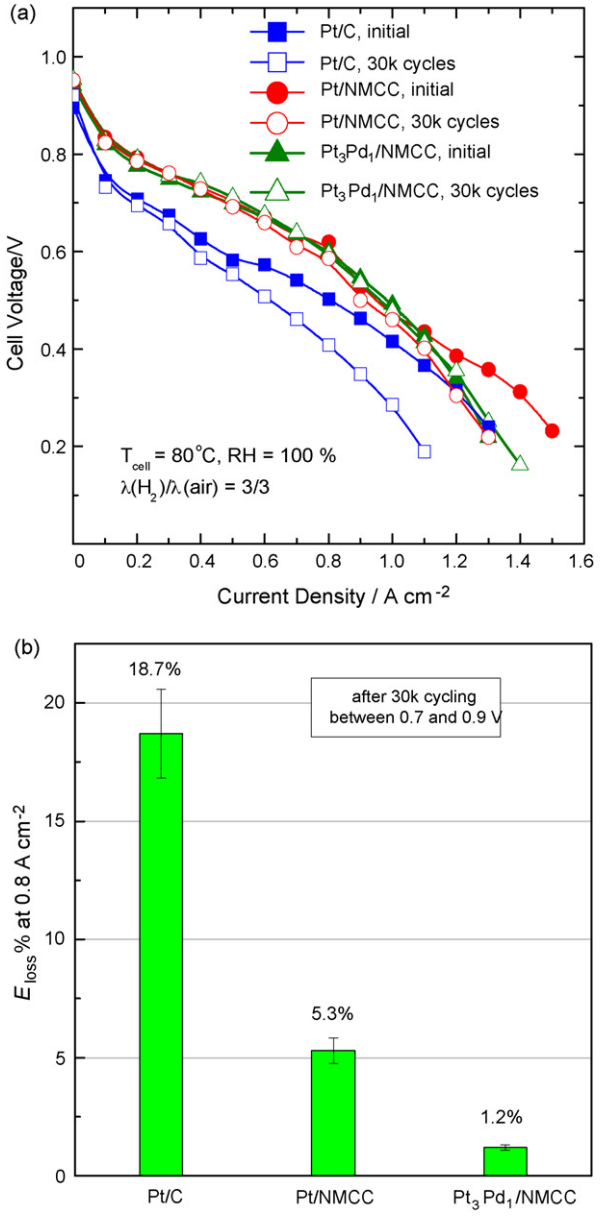

Fig. 9. (a) H_2-air fuel cell polarization curves using the Pt/C catalyst, Pt/NMCC hybrid catalyst, and Pt_3Pd_1/NMCC hybrid catalyst before and after 30,000 cycles of the accelerated stress test on the catalyst. (b) Percentage of fuel cell potential loss at 0.8 A cm^{-2} before and after 30,000 cycles of the accelerated stress test on the catalyst.

Fig. 9a shows the H_2-air fuel cell polarization curves using the Pt/C catalyst, Pt/NMCC hybrid catalyst, and Pt_3Pd_1/NMCC hybrid catalyst before and after 30,000 cycles in the accelerated stress test for catalysts. In the test, the fuel cell cathode is cycled between 0.7 V for 30 s and 0.9 V for 30 s, since Pt sintering and dissolution are accelerated by potential cycling. Fig. 9b shows the percentage of fuel cell potential loss at 0.8 A cm^{-2} before and after 30,000 cycles in the accelerated stress test for catalysts. For accuracy, the error bar is given to the histogram data and the average value of performance loss is also presented in Fig. 9b. After 30,000 cycles, the degree of catalyst degradation decreases from Pt/C (18.7%) to Pt/NMCC (5.3%) to Pt_3Pd_1/NMCC (1.2%). This increased stability is attributed to a synergistic effect from the use of NMCC and Pt, which at least partially results from the formation of a PtCo alloy (as demonstrated by XRD and XPS), and which significantly alleviates the Pt sintering/dissolution. Moreover, the larger particle sizes in the Pt_3Pd_1/NMCC and Pt/NMCC may also contribute to their higher stability than the Pt/C counterpart. The large Pt particles are much more resistant to the Ostwald ripening and particle coalescence occurring during the potential cycling process than the small catalyst particle [13]. The stability of Pt is further improved by doping the hybrid catalysts with a third metal, Pd. Besides the particle size effect, one possible explanation for this increase in stability is the formation of new and more stable PtPdCo ternary alloys revealed by the XRD and XPS characterizations, but the exact reason is still unclear. Further investigations must be performed to determine the origin of the enhanced stability of the Pt_3Pd_1/NMCC hybrid catalyst as compared to the Pt/NMCC hybrid catalyst and the Pt/C catalyst.

Fig. 10 shows the mass activity of the Pt/C catalyst, Pt/NMCC hybrid catalyst, and Pt_3Pd_1/NMCC hybrid catalyst at 0.7 V with the fuel cells operating in relative humidity of 50% and 100% (data is from Figs. 8a and 9a. The mass activity of the different catalysts is calculated with respect to the Pt loading on the fuel cell cathodes. For accuracy, the error bar is given to the histogram data. As shown in Fig. 10, the mass activity of the catalysts in the fuel cells increases from Pt/C to Pt/NMCC to Pt_3Pd_1/NMCC at both relative humidity. This order is not completely consistent with the RDE result: Pt/C < Pt_3Pd_1/NMCC ≤ Pt/NMCC. The reason is unclear now. However, a similar study reported by Ralph and Hogarth on a PtCr catalyst modified with a third metal may shed a light on this issue [50]. They found that the addition of a very small quantity of a third metal in the PtCr catalyst decreases the hydrophilicity of the catalyst, which in turn reduces the retaining water produced by oxygen reduction in the cathode. Consequently, the rate of oxygen permeability in the catalyst layer increases. This may be one of the possibilities in the improved fuel cell performance of the Pt_3Pd_1/NMCC compared to the Pt/NMCC. The effects of hydrophilicity of catalyst on the oxygen diffusion and the resulting mass activity of catalyst in the RDE are negligible due to the employment of thin-film catalyst layer, high electrode rotation speed, and the liquid electrolyte in the RDE measurement. In conclusion, both fuel cell and RDE results demonstrated the higher mass activity of the NMCC-supported Pt and PtPd hybrid catalysts in comparison with the Pt/C due to the alloying effect and particle size effect. Moreover, the nitrogen-containing active sites of the NMCC may also contribute to the overall activity of the hybrid catalysts, which has been evidenced by our on-going study in low Pt loading fuel cells.

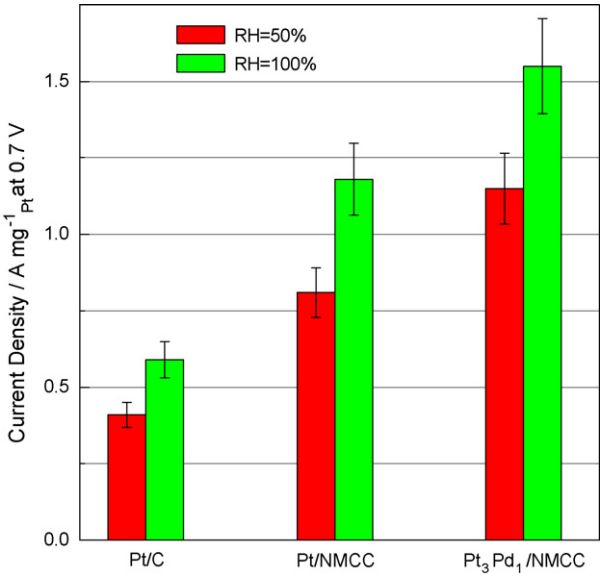

Fig. 10. Mass activity of the Pt/C catalyst, Pt/NMCC hybrid catalyst, and Pt_3Pd_1/NMCC hybrid catalyst at 0.7 V in fuel cells operated at relative humidity of 50% and 100%, respectively.

4. Conclusions

In this work, Pt/NMCC and Pt_3Pd_1/NMCC hybrid catalysts were developed that are composed of a nitrogen-modified carbon composite (NMCC) supporting material, which is itself active for the ORR, instead of a conventional carbon black support. The chemical and physical properties of the catalyst supports and catalysts were characterized by pore size distribution and BET surface area analysis, XRD, XPS, and TEM techniques. The stability of the catalysts was compared using the fuel cell accelerated stress tests (AST) on both the catalyst supports and catalysts. The Pt_3Pd_1/NMCC hybrid catalyst exhibited significantly improved stability when compared to both the Pt/NMCC hybrid catalyst and the Pt/C catalyst. Moreover, both the Pt_3Pd_1/NMCC and Pt/NMCC hybrid catalysts show higher mass activity than the Pt/C catalyst. The alloying effect and particle size effect are involved to the improved stability and mass activity of the hybrid catalysts using a novel support and a third metal additive.

Acknowledgments

The Department of Energy (DE-FG36-08GO88116) and the National Science Foundation Industry/University Cooperative Research Center for Fuel Cells at the University of South Carolina are gratefully acknowledged for their financial support.

References

[1] V. Jalan, E.J. Taylor, J. Electrochem. Soc. 130 (1983) 2299–2302.
[2] B.C. Beard, P.N. Ross, J. Electrochem. Soc. 137 (1990) 3368–3374.
[3] S. Mukerjee, S. Srinivasan, J. Electroanal. Chem. 357 (1993) 201–224.
[4] T. Toda, H. Igarashi, H. Uchida, M. Watanabe, J. Electrochem. Soc. 146 (1999) 3750–3756.
[5] H.R. Colón-Mercado, H. Kim, B.N. Popov, Electrochem. Commun. 6 (2004) 795–799.
[6] P. Yu, M. Pemberton, P. Plasse, J. Power Sources 144 (2005) 11–20.
[7] P.J. Ferreira, G.J. la O', S.-H. Yang, D. Morgan, R. Makharia, S. Kocha, H.A. Gasteiger, J. Electrochem. Soc. 152 (2005) A2256–A2271.
[8] H.R. Colón-Mercado, B.N. Popov, J. Power Sources 155 (2006) 253–263.
[9] S.C. Ball, S.L. Hudson, D. Thompsett, B. Theobald, J. Power Sources 171 (2007) 18–25.
[10] Z. Siroma, K. Ishii, K. Yasuda, Y. Miyazaki, M. Inab, A. Tasaka, Electrochem. Commun. 7 (2005) 1153–1156.
[11] L.M. Roen, C.H. Paik, T.D. Jarvi, Electrochem. Solid-State Lett. 7 (2004) A19–A22.
[12] S. Maass, F. Finsterwalder, G. Frank, R. Hartmann, C. Merten, J. Power Sources 176 (2008) 444–451.
[13] Y. Shao, G. Yin, Y. Gao, J. Power Sources 171 (2007) 558–566.
[14] X. Yu, Siyu Ye, J. Power Sources 172 (2007) 145–154.
[15] M. Shao, K. Sasaki, N.S. Marinkovic, L. Zhang, R.R. Adzic, Electrochem. Coummn. 9 (2007) 2848–2853.
[16] X. Li, S. Ge, C.L. Hui, I.-M. Hsing, Electrochem. Solid-State Lett. 7 (2004) A286–A289.
[17] X. Li, I.-M. Hsing, Electrochim. Acta 51 (2006) 5250–5258.
[18] J.-H. Wee, K.-Y. Lee, S.H. Kima, J. Power Sources 165 (2007) 667–677.

[19] H. Kim, N.P. Subramanian, B.N. Popov, J. Power Sources 138 (2004) 14–24.
[20] G. Faubert, G. Lalande, R. Côté, D. Guay, J.P. Dodelet, L.T. Weng, Electrochim. Acta 41 (1996) 1689–1701.
[21] S.Lj. Gojkovic, S. Gupta, R.F. Savinell, J. Electrochem. Soc. 145 (1998) 3493–3499.
[22] F. Charreteur, F. Jaouen, S. Ruggeri, J.P. Dodelet, Electrochim. Acta 53 (2008) 2925–2938.
[23] E. Yeager, Electrochim. Acta 29 (1984) 1527–1537.
[24] K. Wiesener, Electrochim. Acta 31 (1986) 1073–1078.
[25] S. Maldonado, K.J. Stevenson, J. Phys. Chem. B 109 (2005) 4707–4716.
[26] P.H. Matter, E. Wang, J.-M.M. Millet, U.S. Ozkan, J. Phys. Chem. C 111 (2007) 1444–1450.
[27] N.P. Subramanian, X. Li, V. Nallathambi, S.P. Kumaraguru, H.R. Colon-Mercado, G. Wu, J.-W. Lee, B.N. Popov, J. Power Sources 188 (2009) 38–44.
[28] N.P. Subramanian, S.P. Kumaraguru, H.R. Colón-Mercado, H. Kim, B.N. Popov, T. Black, D.A. Chen, J. Power Sources 157 (2006) 56–63.
[29] V. Nallathambi, J.-W. Lee, S.P. Kumaraguru, G. Wu, B.N. Popov, J. Power Sources 183 (2008) 34–42.
[30] X. Li, H.R. Colon-Mercado, G. Wu, J.-W. Lee, B.N. Popov, Electrochem. Solid State Lett. 10 (2007) B201–B205.
[31] M. Lefèvre, J.P. Dodelet, Electrochim. Acta 48 (2003) 2749–2760.
[32] X. Li, C. Liu, W. Xing, T. Lu, J. Power Sources 193 (2009) 470–476.
[33] K. Kinoshita, Carbon, Electrochemical and Physicochemical Properties, John Wiley & Sons, New York, 1988 (Chapter 6).
[34] G. Wu, D. Li, C. Dai, D. Wang, N. Li, Langmuir 24 (2008) 3566–3575.
[35] Y. Shao, J. Sui, G. Yin, Y. Gao, Appl. Catal. B 79 (2008) 89–99.
[36] S. Mukerjee, J. McBreen, J. Electroanal. Chem. 448 (1998) 163–171.
[37] K.J.J. Mayrhofer, B. Blizanac, M. Arenz, V.R. Stamenkovic, P.N. Ross, N.M. Markovic, J. Phys. Chem. B 109 (2005) 14433–14440.
[38] K. Kinoshita, J. Electrochem. Soc. 137 (1990) 845–848.
[39] J. Perez, E.R. Gonzalez, E.A. Ticianelli, Electrochim. Acta 44 (1998) 1329–1339.
[40] O. Antoine, Y. Bultel, R. Durand, J. Electroanal. Chem. 499 (2001) 85–94.
[41] E. Antolini, Mater. Chem. Phys. 78 (2003) 563–573.
[42] E. Slavcheva, V. Nikolova, T. Petkova, E. Lefterova, I. Dragieva, T. Vitanov, E. Budevski, Electrochim. Acta 50 (2005) 5444–5448.
[43] F.R. Hartley, in: F.R. Hartley (Ed.), Chemistry of the Platinum Group Metals, Elsevier, New York, 1991 (Chapter 1).
[44] M.J. Llorca, J.M. Feliu, A. Aldaz, J. Clavilier, J. Electroanal. Chem. 376 (1994) 151–160.
[45] M. Baldauf, D.M. Kolb, J. Phys. Chem. 100 (1996) 11375–11381.
[46] J. Solla-Gullón, V. Montiel, A. Aldaz, J. Clavilier, Electrochem. Commun. 4 (2002) 716–721.
[47] P.K. Babu, H.S. Kim, J.H. Chung, E. Oldfield, A. Wieckowski, J. Physi. Chem. B 108 (2004) 20228–20232.
[48] X. Li, I.-M. Hsing, Electrochim. Acta 51 (2006) 3477–3483.
[49] H.R. Colón-Mercado, D.T. Hobbs, Electrochem. Commun. 9 (2007) 2649–2653.
[50] T.R. Ralph, M.P. Hogarth, Platinum Met. Rev. 46 (2002) 3–14.